Dalton Transactions

ROYAL SOCIETY OF CHEMISTRY

PAPER

View Article Online
View Journal | View Issue

Cite this: *Dalton Trans.*, 2025, **54**, 3414

Tunable photoluminescence and energy transfer in Dy^{3+} and Eu^{3+} co-doped $NaCaGd(WO_4)_3$ phosphors for pc-WLED applications

Utku Ekim, [a] Ikhlas Kachou, [b] Tarak Kallel,[b,c] Mohamed Dammak, *[b] Miray Çelikbilek Ersundu *[a] and Ali Erçin Ersundu *[a]

Elevated temperatures can lead to reabsorption and color drift, compromising the quality of phosphor-converted white light-emitting diode (pc-WLED) devices. To ensure the performance of WLEDs under these conditions, it is essential to develop luminescent materials that maintain stable color. Consequently, there is a pressing need for single-phase white-emitting phosphors with robust chromatic stability. In this work, we synthesize a series of color-tunable $NaCaGd(WO_4)_3$ (NCGW) phosphors using conventional solid-state reaction method, co-doping with Dy^{3+} and Eu^{3+} in varying ratios. X-ray diffraction, Rietveld refinement and scanning electron microscopy analyses are carried out to identify the phase purity and morphology. The photoluminescence (PL) properties are investigated under excitations of 352 nm and 393 nm. The PL emission spectra and fluorescence decay curves reveal efficient energy transfer between the Dy^{3+} and Eu^{3+} ions within the NCGW host, demonstrating tunable PL emission properties through manipulation of this energy transfer. At elevated temperatures of up to 200 °C, the positions of the characteristic emission peaks of Dy^{3+} and Eu^{3+} in NCGW phosphors remain essentially unchanged. Although the emission band intensities decrease due to thermal quenching, they retain a significant portion of their initial intensity compared to room temperature levels. For proof-of-concept studies, a single-phase NCGW:0.05%Dy^{3+}–0.05%Eu^{3+} phosphor is combined with a commercial 365 nm UV chip to create a WLED device prototype. This prototype achieves a color rendering index of 81.7, a correlated color temperature of 4862 K and Commission International de l'Eclairage chromaticity coordinates of (0.35, 0.37), exhibiting comparable or superior colorimetric values to those reported in previous research. The results indicate that Dy^{3+} and Eu^{3+} co-doped NCGW phosphors, with their high chromaticity stability, have significant potential for full-spectrum WLED applications.

Received 2nd December 2024,
Accepted 18th January 2025

DOI: 10.1039/d4dt03350g

rsc.li/dalton

1. Introduction

With the advancement of lighting technology, phosphor-converted WLEDs (pc-WLEDs) have emerged as the mainstream method for producing white light and are considered the most promising next-generation light sources due to their advantages over traditional incandescent and fluorescent lamps, such as energy efficiency, environmental friendliness, compact size, lightweight, fast response and long lifespan.[1–10] Commercially available pc-WLEDs primarily utilize blue-emitting InGaN chips to excite YAG:Ce^{3+} yellow phosphors. While cost-effective and suitable for mass production, the lack of red emission poses challenges for these pc-WLEDs to achieve warm white light with a low correlated color temperature (CCT) and high color rendering index (CRI), thereby limiting their applicability in areas such as indoor lighting.[11–14] An alternative strategy involves using blue $BaMgAl_{10}O_{17}:Eu^{2+}$, green $(Ba,Sr)_2SiO_4:Eu^{2+}$ and red $(Ca,Sr)AlSiN_3:Eu^{2+}$ phosphors with a UV LED chip. This approach can effectively increase the CRI of the system and provide higher excitation energy, as UV light does not interfere with white light emission.[15–18] However, in addition to the complexity of the production process and the reabsorption behavior of blue emissions by green and red phosphors, the varying aging characteristics and thermal quenching behaviors of mixed tricolor phosphors present challenges in maintaining color balance and chromatic stability for high-quality illumination.[19] Herein,

[a]*Yildiz Technical University, Faculty of Chemical and Metallurgical Engineering, Department of Metallurgical and Materials Engineering, Glass Research and Development Laboratory, Istanbul, 34220, Türkiye. E-mail: ersundu@yildiz.edu.tr*
[b]*Laboratoire de Physique Appliquée, Groupe de Physique des Matériaux Luminescents, Faculté des Sciences de Sfax, Département de Physique, Université de Sfax, BP 1171, Sfax, Tunisia. E-mail: madidammak@yahoo.fr*
[c]*Department of Physics, College of Science and Arts, Jouf University, Al-Qurayyat Branch, P.O. Box 756, Al-Qurayyat 77425, Saudi Arabia*

developing single-phase white-emitting phosphors with stable emission across a wide temperature range would be a highly desirable solution to these challenges, as such phosphors can combine the benefits of high chromatic quality and stable color performance without the drawbacks associated with mixing multiple phosphors. Therefore, in recent years, significant effort has been dedicated to single-phase white-emitting phosphors incorporating single or multiple lanthanide activators as an alternative method for producing high-quality WLEDs.[1–4,15–19]

Trivalent lanthanide activators exhibit unique optical properties, including narrow and intense luminescence, long lifetimes, emissions spanning the entire visible spectrum (red, green and blue) and excellent thermal and chemical stability.[20,21] Dy^{3+} among trivalent lanthanide activators exhibits three emission bands in the visible region: blue (~480 nm), yellow (~575 nm) and red (~665 nm), attributed to the $^4F_{9/2} \rightarrow {}^6H_{15/2}$, $^4F_{9/2} \rightarrow {}^6H_{13/2}$ and $^4F_{9/2} \rightarrow {}^6H_{11/2}$ transitions, respectively.[22] Consequently, Dy^{3+} ions are widely utilized in the development of single-phase white-emitting phosphors due to their well-insulated 4f orbit by the 5d and 6s orbits, which ensures that the energy levels are rarely affected by the surrounding environment; notably, there are two excitation peaks at around 350 and 450 nm that correspond to existing LED chips, suggesting their potential use as components in pc-WLEDs. However, akin to the limitations of the blue chip + YAG:Ce^{3+} yellow phosphor system, the white light generated by Dy^{3+} ions is constrained by their weak red emissions, resulting in low CRI and high CCT values, which are insufficient on their own. To enhance their emission properties, various red-emitting lanthanides such as Eu^{3+}, Pr^{3+} and Sm^{3+} can be co-doped with Dy^{3+} ions. Among these, Eu^{3+} ions are particularly notable for their strong red emission characterized by a maximum peak around 613 nm attributed to the $^5D_0 \rightarrow {}^7F_2$ transition. This emission property has the potential to address the deficiency of the red component in the emission spectra of Dy^{3+} ions. However, with its highest excitation peak situated at ~395 nm, the improper excitation position of Eu^{3+}-doped phosphors usually limits their practical use in pc-WLED applications.[23–26] Herein, Dy^{3+} ions can effectively act as sensitizers for Eu^{3+}, facilitating energy transfer. Therefore, when Dy^{3+} is co-doped into Eu^{3+}-activated phosphors as a sensitizer, red emission can be effectively realized and excited by near UV or UV chips.[27,28]

The chemical and physical characteristics of host materials (*i.e.*, phosphors) play a critical role in determining luminescent performance. Host materials with a wide energy band gap (>3.3 eV) are preferred for accommodating lanthanides, as they enable efficient radiative transitions at luminescent centers while minimizing emission losses at high temperatures.[29] Consequently, careful selection of suitable phosphor hosts is essential, as it significantly impacts the luminescent performance and stability of the phosphors. In recent years, tungstate phosphors have attracted considerable attention due to their excellent photoluminescence (PL) properties, chemical stability, and ability to support multiple-ion doping.[27] The NCGW matrix is particularly well-suited for lanthanide activators because of its wide energy band gap, which minimizes emission losses at high temperatures and ensures efficient radiative transitions for lanthanides. Additionally, the WO_4 group within NCGW acts as an effective sensitizer, transferring absorbed near-UV light to the lanthanide ions, thereby enhancing their absorption efficiency and boosting the luminescent performance of lanthanide ions.[30,31] This makes NCGW an ideal candidate for achieving stable and tunable PL properties.

While research on NCGW phosphors has been relatively limited, several studies have demonstrated the potential of this matrix for various applications. For instance, Wang *et al.* reported red-emitting NCGW phosphors doped with Eu^{3+} synthesized *via* the hydrothermal method.[30] Similarly, Xie *et al.* explored the PL properties of Tb^{3+}-doped and Tb^{3+}, Eu^{3+} co-doped NCGW phosphors for color display devices and pc-WLEDs.[31] However, to the best of our knowledge, the luminescence properties of Dy^{3+} and Eu^{3+} co-doped NCGW phosphors for pc-WLED applications have not yet been reported. Therefore, in this study, we synthesize Dy^{3+} and Eu^{3+} co-doped NCGW phosphors using a conventional solid-state reaction method to explore their tunable PL and energy transfer mechanisms. The phase purity and morphology are determined through X-ray diffraction (XRD), Rietveld refinement and scanning electron microscopy (SEM) analyses. The effective energy transfer is systematically evaluated using PL spectra and fluorescence decay curves, revealing a wide range of emission colors by adjusting the Dy^{3+} and Eu^{3+} doping ratios. Temperature-dependent PL spectra are recorded to assess luminescence intensity and colorimetric properties at elevated temperatures. Ultimately, a prototype WLED device, fabricated with a selected phosphor and a 365 nm UV chip, demonstrate outstanding performance, indicating that Dy^{3+} and Eu^{3+} co-doped NCGW phosphors have significant potential for pc-WLED applications.

2. Experimental studies

2.1. Synthesis of Dy^{3+}/Eu^{3+} co-doped $NaCaGd(WO_4)_3$ phosphors

A series of NCGW: xDy^{3+}–yEu^{3+} (x = 0–0.15; y = 0–0.07 in mol%) phosphors is prepared by through conventional solid-state reactions, using Na_2CO_3, $CaCO_3$, Gd_2O_3 and WO_3 along with Dy_2O_3 and Eu_2O_3. All raw materials, of analytical grade, are used as received without further purification. These compounds are weighed in stoichiometric ratios and thoroughly ground for 30 minutes in an agate mortar to achieve uniformity. The mixture is then placed in an alumina crucible and preheated at 400 °C in a muffle furnace for 6 hours, followed by regrinding. To obtain the target material in its pure phase, the mixture is sintered at 800 °C for 4 hours. Finally, the products are cooled to room temperature by switching off the muffle furnace and the sample is ground into a fine powder. We confirm that all samples are sintered in ambient atmospheric conditions, which are known to favor and stabilize the Eu^{3+}

oxidation state due to the presence of oxygen. Under these conditions, europium ions predominantly exist in the Eu^{3+} state, minimizing the possibility of Eu^{2+} formation.

2.2. Fabrication of pc-WLED device

The prototype WLED device is fabricated by combining the selected NCGW:0.05%Dy^{3+}–0.05%Eu^{3+} phosphor with a commercial 365 nm UV chip. The phosphor and epoxy resin are mixed in a 1 : 5 ratio and thoroughly blended for about 15 minutes. The resulting mixture is dried at 120 °C and then coated onto the UV chip to fabricate the WLEDs.

2.3. Characterization studies

The phase purity of the synthesized phosphors is examined using XRD measurements conducted with a Rigaku Ultima IV diffractometer employing Cu Kα radiation (λ = 1.5406 Å). The XRD peak positions and intensities are compared against the corresponding ICDD card files. The morphological properties and elemental mapping are analyzed with a Thermo Scientific Apreo 2 S LoVac field emission scanning electron microscope (FE-SEM) operating at a working voltage of 10 kV and a resolution of 0.8 nm. Infrared spectroscopic analysis is performed using a PerkinElmer FTIR-100 spectrophotometer, covering the wavenumber range of 400 cm^{-1} to 4000 cm^{-1}. The steady-state and time-resolved PL properties of the phosphors are investigated using an Edinburgh Instruments FS5 spectrofluorometer equipped with a 150W xenon lamp as the excitation source with a high spectral resolution. Photoluminescence quantum yield (PLQY) measurements are performed using an integrating sphere with a 150 mm internal cavity coated with polytetrafluoroethylene. The measurements are carried out under a 360 nm excitation wavelength, ensuring a signal-to-noise ratio exceeding 6000 : 1 for the water Raman signal and a spectral resolution of 0.5 nm. Colorimetric properties such as the Commission Internationale de l'E'clairage (CIE) 1931 color coordinates, CCT and CRI are determined by using OSRAM Color Calculator software. Time-resolved lifetime spectra are measured with the same spectrofluorometer utilizing a time-correlated single-photon counting (TCSPC) technique, equipped with a microsecond xenon lamp as the excitation source. The decay curves are fitted with a bi-exponential equation:

$$I(t) = A_1 e^{\left(\frac{-t}{\tau_1}\right)} + A_2 e^{\left(\frac{-t}{\tau_2}\right)} \quad (1)$$

where, $I(t)$ represents emission intensity, τ_1 and τ_2 are the measured lifetime values and A_1 and A_2 are decay constants. The Measured lifetime value (τ_{meas}) for each transition is calculated by using the following expression:

$$\tau_{meas} = \frac{A_1\tau_1^2 + A_2\tau_2^2}{A_1\tau_1 + A_2\tau_2} \quad (2)$$

The choice of a bi-exponential fit for the decay curves is based on the assumption that luminescence decay involves two distinct processes or emission sites with different lifetimes, a common occurrence in doped materials. In our synthesized samples, we find that the bi-exponential model best fits the experimental data, as confirmed by analyzing fitting residuals and reduced chi-square values.

The temperature dependence of the PL properties is studied using a Pike Technologies heated solid transmission attachment fitted to the spectrofluorometer, enabling measurements over a temperature range from room temperature to 200 °C.

3. Results and discussion

3.1. Crystal structure, morphology and phase characterization

The XRD patterns for undoped NCGW, NCGW:0.05%Dy^{3+} and NCGW:0.05%Eu^{3+} single-doped and NCGW:0.05%Dy^{3+}–0.05% Eu^{3+} co-doped phosphors are shown in Fig. 1a. The diffraction patterns align closely with those of the $CaWO_4$ reference (ICDD # 04-007-9496), with no secondary phases or contaminants detected. This similarity suggests that Dy^{3+} (r = 0.91 Å, CN = 6) and Eu^{3+} (r = 0.95 Å, CN = 6) ions successfully incorporate into the NCGW lattice by substituting Gd^{3+} (r = 0.94 Å, CN = 6) ions due to their similar ionic radii. It should be noted, however, that NCGW and $CaWO_4$ have distinct crystal structures; $CaWO_4$ is referenced here solely as a comparative standard for diffraction patterns. The primary structural difference between NCGW and $CaWO_4$ lies in their composition and resulting lattice characteristics. While both materials share a scheelite-like structural framework, $CaWO_4$ is a simple binary compound crystallizing in the $I4_1/a$ tetragonal space group, where Ca^{2+} and WO_4^{2-} ions occupy highly symmetric lattice sites. In contrast, NCGW is a more compositionally complex phase, incorporating Na^+, Ca^{2+}, and Gd^{3+} ions that share cationic lattice sites. This compositional complexity introduces subtle distortions within the lattice due to the variations in cation sizes and charges, though the scheelite-like backbone remains the dominant feature of the crystal structure.

The right panel of Fig. 1a shows the magnified primary diffraction peak for the (112) lattice plane of the phosphors, alongside the characteristic diffraction peak of $CaWO_4$. Notably, incorporating 0.05% Dy^{3+} into the NCGW host shifts the main XRD peak toward larger diffraction angles, due to the smaller radii of Dy^{3+} ions compared to Gd^{3+} ions, causing lattice shrinkage. A slight shift is also observed with 0.05% Dy^{3+}–0.05% Eu^{3+} co-doping. However, no significant peak shift occurs with 0.05% Eu^{3+} doping, given the close ionic radius values of Eu^{3+} and Gd^{3+}. Thus, it can be concluded that the solid-state reaction effectively synthesizes single-phase phosphors doped with Dy^{3+} and Eu^{3+} ions in NCGW host.

To further validate the NCGW host lattice structure and ensure accurate phase identification, the selected NCGW:0.05%Dy^{3+}–0.05%Eu^{3+} co-doped phosphor is subjected to XRD Rietveld refinement using the FullProf_Suite program. The refined cell parameters show strong alignment with previously reported NCGW structural data.[31] Refinement factors of R_p = 7.74%, R_{wp} = 9.86% and χ^2 = 1.822 indicate a high-

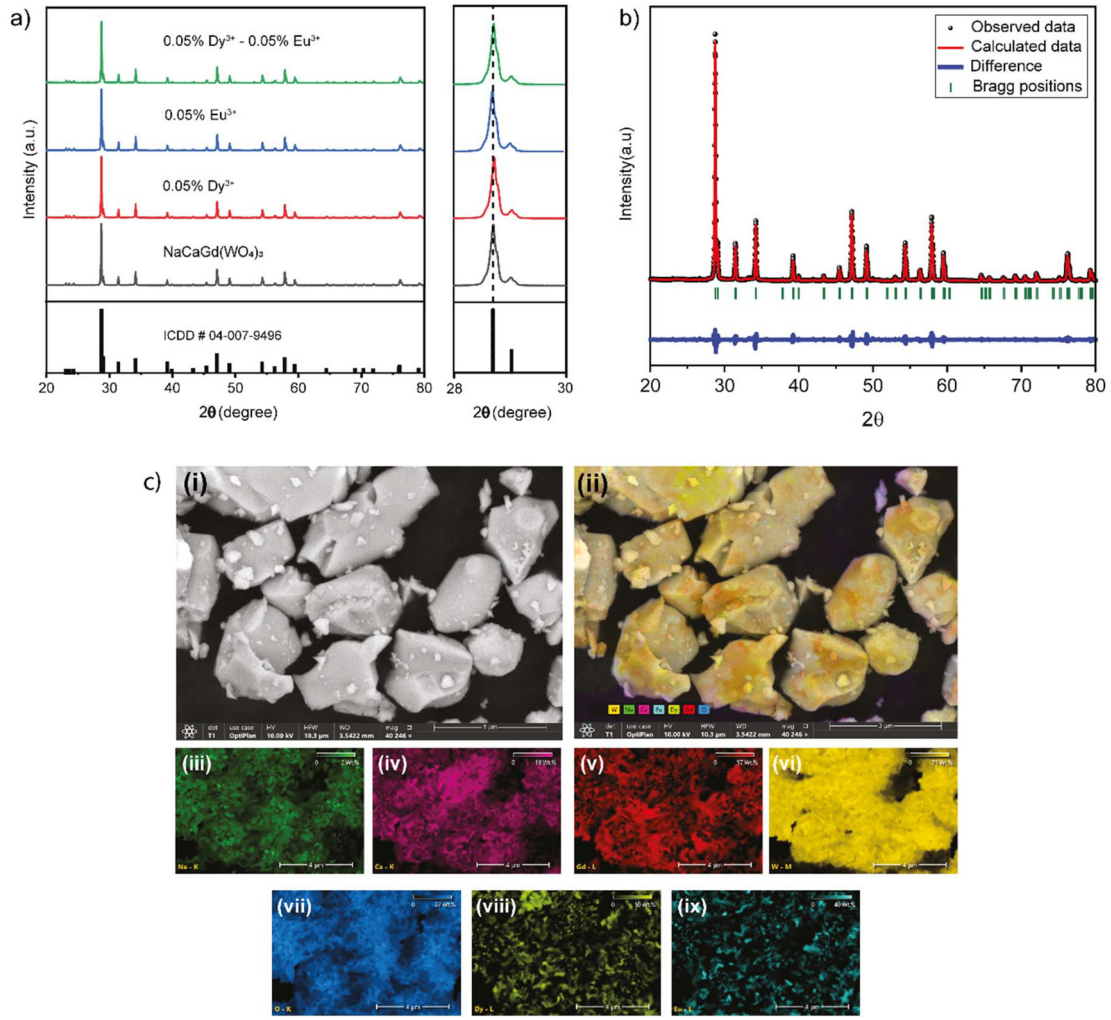

Fig. 1 (a) XRD patterns of the undoped NCGW, NCGW:0.05%Dy^{3+} and NCGW:0.05%Eu^{3+} single-doped and NCGW:0.05%Dy^{3+}–0.05%Eu^{3+} co-doped phosphors. (b) Rietveld refinement for the representative NCGW:0.05%Dy^{3+}–0.05%Eu^{3+} co-doped phosphor. (c) (i) FE-SEM image of the representative NCGW:0.05%Dy^{3+}–0.05%Eu^{3+} co-doped phosphor, (ii) Overall distribution of detected elements, (iii)–(ix) Distribution of Na, Ca, Gd, W, O, Dy and Eu, respectively.

quality fit, confirming the target crystal structure as NCGW and supporting the integrity of subsequent analyses based on this verified structure.

The NCGW:0.05%Dy^{3+}–0.05%Eu^{3+} co-doped sample is further examined for its morphology. The FE-SEM image in Fig. 1c(i) shows that the synthesized phosphors have an irregular morphology with particle sizes around 2–3 μm. Elemental distribution is analyzed *via* FE-SEM mapping. Fig. 1c(ii) presents the overall distribution of elements, while Fig. 1c(iii)–(ix) illustrate the specific distributions of Na, Ca, Gd, W, O, Dy and Eu. The homogeneous distribution of all elements confirms the efficient doping of Dy^{3+} and Eu^{3+} ions.

3.2. Infrared spectra, diffuse reflectance and optical band gap analysis

Infrared spectroscopy is used to study the absorption bands and their vibration frequencies. Fig. 2a shows the infrared spectra for undoped NCGW, NCGW:0.05%Dy^{3+} and NCGW:0.05%Eu^{3+} single-doped and NCGW:0.05%Dy^{3+}–0.05%Eu^{3+} co-doped phosphors. The spectra display a broad, strong band between 480 cm^{-1} and 900 cm^{-1} (highlighted with a blue background in Fig. 3a), which is attributed to the vibrations of the WO_4 units. Additionally, peaks at 840 cm^{-1} and 928 cm^{-1} (highlighted with a yellow background in Fig. 3a) correspond to the asymmetric stretching vibrations of the W–O units and the symmetric stretching vibrations of W–O–W in WO_4 units, respectively.[32] The sharp peak observed at 445 cm^{-1} (highlighted with a green background in Fig. 3a) corresponds to the Gd–O stretching vibrations.[33]

The diffuse reflectance (DR) spectra of NCGW, NCGW:0.05%Dy^{3+} and NCGW:0.05%Eu^{3+} single-doped and NCGW:0.05%Dy^{3+}–0.05%Eu^{3+} co-doped phosphors are shown in Fig. 2b. All samples display a broad absorption band between 250 to 450 nm, which is attributed to the charge

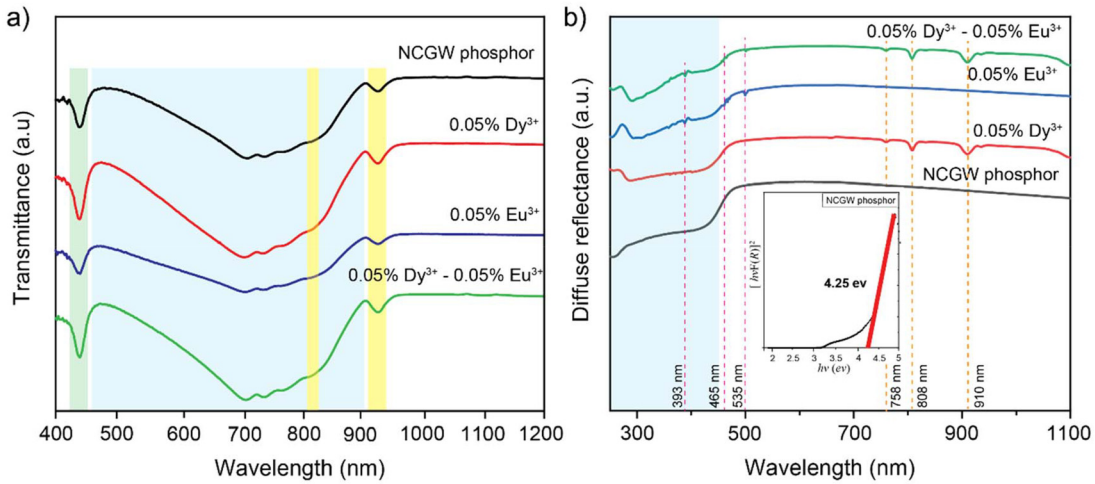

Fig. 2 (a) Infrared spectra, and (b) diffuse reflectance spectra of undoped NCGW, NCGW:0.05%Dy^{3+} and NCGW:0.05%Eu^{3+} single-doped and NCGW:0.05%Dy^{3+}–0.05%Eu^{3+} co-doped phosphors. (Inset of b shows the band gap of undoped NCGW phosphor).

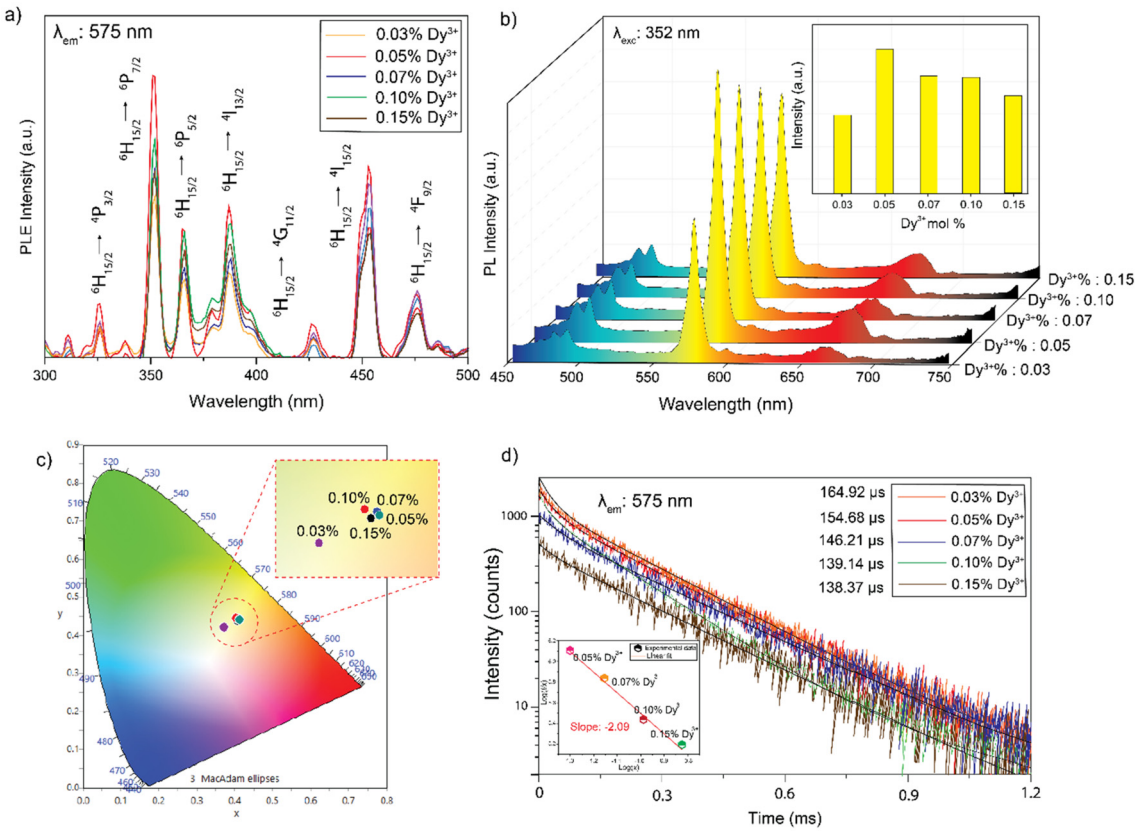

Fig. 3 (a) PLE spectra for 575 nm emission, (b) PL spectra under 352 nm excitation, (c) corresponding CIE coordinates, (d) decay curves of NCGW: $x$$Dy^{3+}$ (x = 0.03, 0.05, 0.07, 0.10, 0.15 mol%) phosphors. (Inset of Fig. 1b illustrates the relationship between yellow emission intensity (575 nm) and Dy^{3+} concentration and inset of Fig. 1d shows the plot of log(I/x) *vs.* log(x)).

transfer transition from the 2p state of O to the 5d state of W. In the DR spectrum of the NCGW:0.05%Dy^{3+} single-doped phosphor and NCGW:0.05%Dy^{3+}–0.05%Eu^{3+} co-doped phosphor, the absorption peaks appearing at 758, 808 and 910 nm correspond to the transitions of Dy^{3+} ions, originating from its ground state $^6H_{15/2}$ to the excited states $^6F_{3/2}$ ($^6F_{1/2}$), $^6F_{5/2}$ and $^6F_{7/2}$, respectively.[34] In addition, the DR spectra of the NCGW:0.05%Eu^{3+} single-doped phosphor and NCGW:0.05%

Dy^{3+}–0.05%Eu^{3+} co-doped phosphor exhibit characteristic Eu^{3+} absorption peaks at 393, 465, and 535 nm, corresponding to the transitions $^7F_0 \rightarrow {}^5L_6$, $^7F_0 \rightarrow {}^5D_2$, and $^7F_1 \rightarrow 5D_1$, respectively.[31]

The optical band gap (E_g) value is a crucial factor in determining the efficient luminescence properties of activators in a host material. Therefore, E_g value of undoped NCGW phosphor is determined from the DR spectra using Kubelka–Munk absorption function $F(R)$ using the following equation:[35,36]

$$F(R) = (1 - R)^2/(2R) \quad (3)$$

and analyzed using the Tauc equation:

$$[h\nu F(R)]^n = A(h\nu - E_g) \quad (4)$$

where R represents the diffuse reflectance coefficient, $h\nu$ is the photon energy, n determines the nature of the band gap (n = 2 for a direct band gap and n = 1 for an indirect band gap), and A is the absorption constant. By plotting $(h\nu F(R))^2$ *versus* $h\nu$, a linear region is observed, confirming that n = 2, which indicates a direct band gap. From this analysis, the undoped NCGW phosphor is found to have a direct E_g of 4.25 eV (inset of Fig. 2b). This wide direct band gap highlights its suitability as a host for lanthanide doping, enabling efficient radiative transitions at luminescent centers.

3.3. Photoluminescence characteristics of $NaCaGd(WO_4)_3$: Dy^{3+} phosphors

PLE measurements are conducted at a monitoring wavelength of 575 nm, where the maximum PL peak is observed, due to the characteristic transition ($^6H_{15/2} \rightarrow {}^4F_{9/2}$) of Dy^{3+} ions doped at various concentrations (0.03, 0.05, 0.07, 0.10, 0.15 mol%) into the NCGW structure, as shown in Fig. 3a. Unlike other Dy^{3+} and Eu^{3+} co-doped phosphors, the NCGW host does not exhibit a broad band associated with the charge transfer band upon single Dy^{3+} doping.[27,28] However, multiple excitation wavelengths in the 300–500 nm range correspond to the characteristic transitions of Dy^{3+} ions, with peak positions remaining consistent across different Dy^{3+} doping concentrations. The identified excitation wavelengths corresponding to the f–f electronic transitions of Dy^{3+} ions are 327 nm ($^6H_{15/2} \rightarrow {}^4P_{3/2}$), 352 nm ($^6H_{15/2} \rightarrow {}^4P_{7/2}$), 365 nm ($^6H_{15/2} \rightarrow {}^6P_{5/2}$), 388 nm ($^6H_{15/2} \rightarrow {}^4I_{13/2}$), 427 nm ($^6H_{15/2} \rightarrow {}^4G_{11/2}$), 453 nm ($^6H_{15/2} \rightarrow {}^4I_{15/2}$) and 476 nm ($^6H_{15/2} \rightarrow {}^4F_{9/2}$). The transition from $^6H_{15/2} \rightarrow {}^4P_{7/2}$ at 352 nm exhibits the highest intensity. Therefore, this transition wavelength is selected to be used for excitation in PL measurements.

PL analysis excited at 352 nm is performed on NCGW samples with varying Dy^{3+} concentrations. The results, shown in Fig. 3b, exhibit the characteristic emissions of Dy^{3+} ions at 480 nm (blue), 575 nm (yellow) and 665 nm (red), corresponding to the typical $^4F_{9/2} \rightarrow {}^6H_{15/2}$ electric dipole transition, $^4F_{9/2} \rightarrow {}^6H_{13/2}$ magnetic dipole transition and $^4F_{9/2} \rightarrow {}^6H_{11/2}$ transition. As observed, the intensity of the yellow emission is significantly higher than that of the other two emissions. This indicates that Dy^{3+} is located at a low-symmetry site without an inversion center, as the hypersensitive electric dipole transition, rather than the magnetic dipole transition, is strongly influenced by the surrounding environment.[37]

While the Dy^{3+} concentrations do not affect the positions of the PL peaks, they significantly influence the intensity of these emissions. The inset in Fig. 3b illustrates the relationship between Dy^{3+} concentration and PL intensity at 575 nm. The emission intensity initially increases up to 0.05% Dy^{3+} and then decreases with further increases in concentration. This decrease is attributed to the effect of concentration quenching. Consequently, the sample with 0.05% Dy^{3+} is selected as the optimal doping concentration due to its maximum emission intensity.

In Fig. 3c, a CIE diagram illustrates how the emission coordinates change with different Dy^{3+} concentrations. The sample with 0.03% Dy^{3+} has emission characteristics closest to the white region, whereas higher doping levels shift the emission towards the yellow region, with no significant differences observed among them.

Fig. 3d presents the lifetime analysis by monitoring the 575 nm emission under the excitation of 352 nm for samples with varying Dy^{3+} concentrations. Consistent with literature findings, an increase in Dy^{3+} concentration correlates with shorter lifetimes due to the concentration quenching. Concentration quenching arises from non-radiative energy transfer mechanisms among luminescent centers, which encompass exchange interaction, radiative reabsorption and electric multipolar interactions. To determine the specific mechanism between Dy^{3+} ions, the critical distance (R_c) is calculated using the following equation proposed by Blasse *et al.*:[38]

$$R_c = 2\left(\frac{3V}{4\pi X_c N}\right)^{1/3} \quad (5)$$

where V represents the volume of the unit cell, X_c stands for the critical concentration for which emission reaches a maximum and N refers to the number of formula units per unit cell. For NCGW:Dy^{3+} phosphors, using V = 312.53 Å^3, X_c = 0.05 and N = 4, the calculated critical distance is 14.4 Å. This may rule out the exchange interaction since it happens often when the R_c value between activators is less than 5. The radiative absorption process needs a significant overlap between the excitation and emission spectra, which is unlikely to occur in this system. According to the aforementioned calculations, the predominant energy-transfer mechanism between Dy^{3+} in the current system will be the electric multipolar interaction. The following formula is further used to determine the exact item.[39,40]

$$\frac{I}{x} = \left[1 + \beta(x)^{\frac{\theta}{3}}\right]^{-1} \quad (6)$$

where I, x and β represent the emission intensity, Dy^{3+} concentration beyond the critical content and a constant for a specific host under the same excitation circumstances, respectively. θ = 6, 8 and 10 corresponds to the electric dipole–dipole, dipole–

quadrupole and quadrupole–quadrupole interactions, respectively. The correlation of $\log(I/x)$ *vs.* $\log(x)$ is presented with a linear fit, as shown in inset of Fig. 3d. The slope of the fitted line is −2.09, which corresponds to $-\theta/3$. Therefore θ = 6.27, which is closest to 6, suggesting that the energy-transfer mechanism between Dy^{3+} in the NCGW:Dy^{3+} phosphors is mediated by electric dipole–dipole interaction.

3.4. Photoluminescence characteristics of $NaCaGd(WO_4)_3$: Dy^{3+}–Eu^{3+} phosphors and energy transfer mechanisms

After establishing the optimal Dy^{3+} ion concentration at 0.05%, Eu^{3+} ions are introduced to the NCGW host in varying concentrations (0.005–0.07%) while keeping Dy^{3+} doping level constant. The results of the PL analysis, excited at 393 nm—the most sensitive excitation wavelength for Eu^{3+} ions—are shown in Fig. 4a. As shown in the graph, increasing the Eu^{3+} concentration does not shift the peak positions; however, the PL intensity increases with the increment of Eu^{3+} concentration.

The inset in Fig. 4a shows the variation of the characteristic red emission peak at 613 nm with different Eu^{3+} concentrations. The impact of these changes in emission peaks is clearly depicted in the CIE diagram in Fig. 4b, where the emission colors shift from the orange to the red region. This demonstrates that the emission color can be tuned by simply adjusting the Eu^{3+} concentration.

The inset of Fig. 4a illustrates the relationship between red emission intensity (613 nm) and Eu^{3+} concentration, while Fig. 4d shows the relationship between yellow (575 nm) and red (613 nm) emission intensities and Eu^{3+} concentration. In Fig. 4a and c, NCGW:0.05% Eu^{3+} and NCGW:0.05%Dy^{3+} single-doped phosphors are shown with dashed lines to compare Dy^{3+}-free and Eu^{3+}-free phosphors with those containing varying Dy^{3+} and Eu^{3+} concentrations, respectively.

Fig. 4c presents the PL analysis results when the excitation wavelength is changed to 352 nm, which is most sensitive for Dy^{3+} ions. The graph shows that the characteristic Dy^{3+} emissions at 472 nm ($^6H_{15/2} \rightarrow {}^4P_{3/2}$) and 510 nm ($^6H_{15/2} \rightarrow {}^4P_{3/2}$) in the Eu^{3+}-free phosphor are affected by the introduction of Eu^{3+} ions through energy transfer between Dy^{3+} and Eu^{3+} ions, resulting in a decrease in PL intensity. The inset in Fig. 4c details the changes in the characteristic Dy^{3+} emission at 575 nm and the Eu^{3+} emission at 613 nm with varying Eu^{3+} concentrations. Upon excitation at 352 nm, the presence of the Eu^{3+} ion peak at 613 nm indicates the energy transfer between Dy^{3+} and Eu^{3+} ions. The change in emission colors with 352 nm excitation is depicted in Fig. 4d, showing that increasing Eu^{3+} concentration causes the emission color to slightly shift towards the orange region.

Fig. 4e presents the lifetime measurement performed with an excitation wavelength of 352 nm, targeting Dy^{3+} ions, and an emission wavelength of 613 nm, characteristic of Eu^{3+} ions. As the Eu^{3+} ion concentration increases while maintaining a constant Dy^{3+} ion concentration, the average lifetime decreases slightly (from 182.32 μs to 177.18 μs). This decrease is due to enhanced energy transfer from Dy^{3+} to Eu^{3+} ions and additional non-radiative decay pathways, such as cross-relaxation and energy migration among Eu^{3+}ions, at higher Eu^{3+}concentrations. This behavior aligns with previous studies and confirms efficient energy transfer dynamics.[27,41]

To better investigate the energy transfer between Dy^{3+} and Eu^{3+} ions in the NCGW phosphor host, PLE spectra of NCGW:0.05% Dy^{3+} and NCGW:0.05%Eu^{3+} single-doped and NCGW:0.05% Dy^{3+}–0.05%Eu^{3+} co-doped phosphors are monitored, as shown in Fig. 5a. Initially, as evident from Fig. 5a (top), both NCGW:0.05%Dy^{3+} single-doped and NCGW:0.05% Dy^{3+}–0.05%Eu^{3+} co-doped phosphors are examined to observe the excitation behavior of Dy^{3+} ions at their optimal PL emission wavelength of 575 nm. The PLE results at 575 nm indicate that adding Eu^{3+} does not affect the sensitive excitation bands of Dy^{3+} ions, suggesting no energy transfer occurs from Eu^{3+} ions to Dy^{3+} ions. Additionally, inset of Fig. 5a illustrates PL emission graph for NCGW:0.05%Eu^{3+} sample at 352 nm excitation representing that the emission peaks obtained are at very low count values and within the noise levels, suggesting that an additional mechanism, *i.e.*, energy transfer from Dy^{3+} ions to Eu^{3+} ions, is responsible for enabling the emission peak at 613 nm. For comprehensive comparison, the same experiment is conducted on NCGW:0.05%Eu^{3+} single-doped and NCGW:0.05%Dy^{3+}–0.05%Eu^{3+} co-doped phosphors, as given in Fig. 5a (bottom). PLE analysis at 613 nm, specific to Eu^{3+} ions, reveals characteristic excitation wavelengths of Eu^{3+} ions at 320 nm ($^7F_0 \rightarrow {}^5H_6$), 362 nm ($^7F_0 \rightarrow {}^5D_4$), 380 nm ($^7F_0 \rightarrow {}^5L_7$), 393 nm ($^7F_0 \rightarrow {}^5L_6$), 415 nm ($^7F_0 \rightarrow {}^5D_3$) and 465 nm ($^7F_0 \rightarrow {}^5D_2$). However, in the NCGW:0.05%Dy^{3+}–0.05% Eu^{3+} co-doped phosphor, two additional peaks are observed at 352 nm ($^6H_{15/2} \rightarrow {}^6P_{7/2}$) and 455 nm ($^6H_{15/2} \rightarrow {}^4I_{15/2}$), which are characteristic transitions of Dy^{3+} ions. These additional peaks in the PLE analysis at 613 nm indicate unidirectional energy transfer from Dy^{3+} ions to Eu^{3+} ions.

To further elucidate the energy transfer between Dy^{3+} and Eu^{3+} ions, the excitation and emission spectra of NCGW:0.05% Eu^{3+} and NCGW:0.05%Dy^{3+} phosphors are recorded, as shown in Fig. 5b. The excitation spectrum of NCGW:0.05%Eu^{3+} overlaps with the emission spectrum of NCGW:0.05%Dy^{3+}. Specifically, the spectral overlap between the $^7F_0 \rightarrow {}^5D_2$ transition (excitation) of Eu^{3+} and the $^4F_{9/2} \rightarrow {}^6H_{15/2}$ transition (emission) of Dy^{3+} ions strongly suggests the feasibility of energy transfer from Dy^{3+} to Eu^{3+}. This observation provides further evidence supporting energy migration between the two ions.

In addition, unlike the Dy^{3+} single-doped NCGW phosphors, the introduction of Eu^{3+} ions causes the NCGW host to exhibit a broad band at around 287 nm, as shown in Fig. 5c. Therefore, to gain a deeper understanding of the potential energy transfers between lanthanide ions (Dy^{3+} and Eu^{3+}) and the phosphor host, a schematic energy level diagram is shown in Fig. 5d. The PLE analysis reveals that excitation at 287 nm excites Eu^{3+} ions in the NCGW:0.05%Dy^{3+}–0.05%Eu^{3+} co-doped phosphor, leading to emissions at 613 nm. This indicates that the NCGW phosphor host effectively transfers energy to the doped Eu^{3+} ions. This finding serves as a foun-

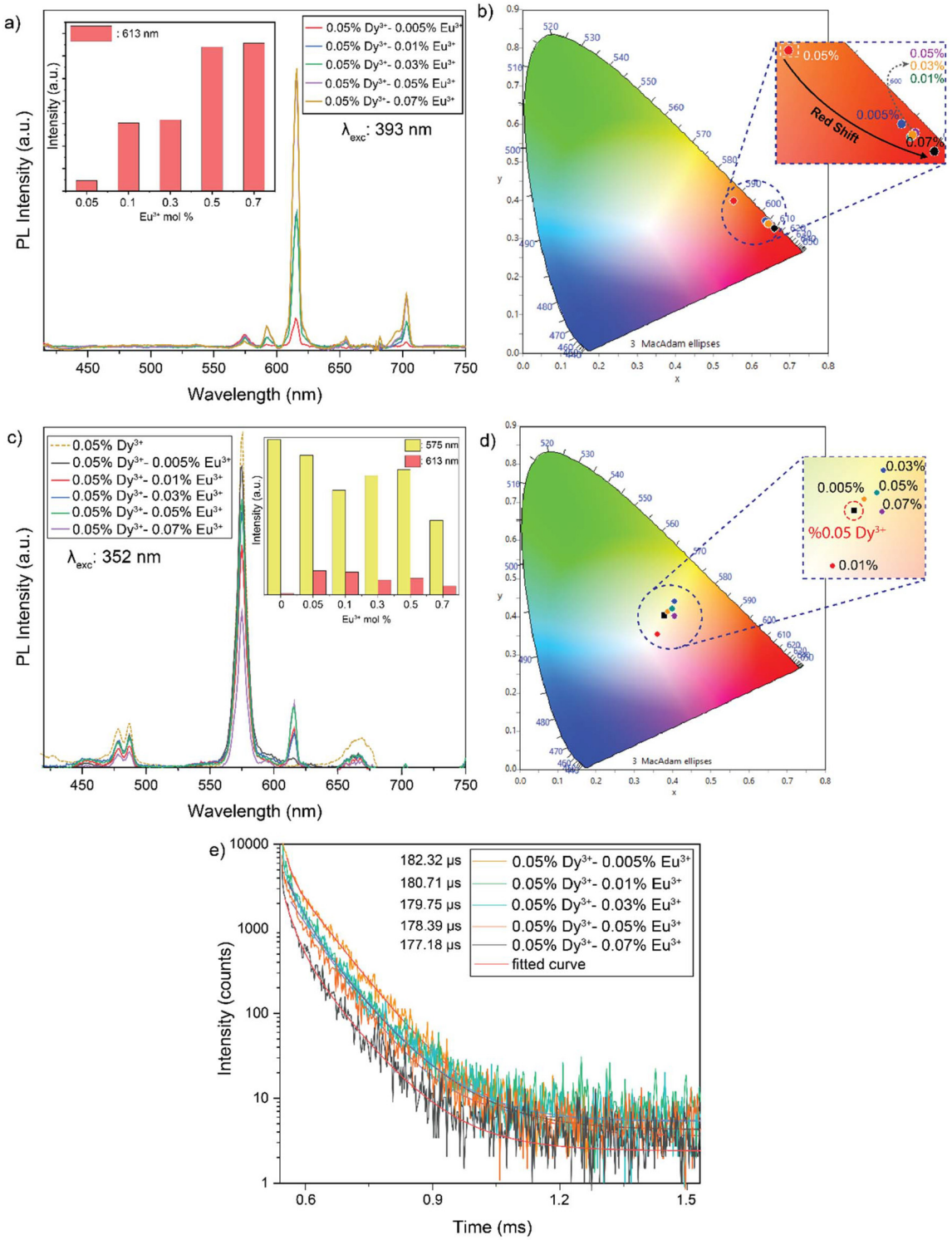

Fig. 4 (a) and (c) PL spectra and (b) and (d) corresponding CIE coordinates of NCGW:0.05%Dy^{3+}–*y*Eu^{3+} phosphors under excitation with (a) and (b) 393 nm and (c) and (d) 352 nm, respectively, (e) decay curves of NCGW:0.05%Dy^{3+}–*y*Eu^{3+} (*y* = 0.005, 0.01, 0.03, 0.5, 0.7 mol%) phosphors.

dation for the energy level diagram, illustrating that upon 287 nm excitation, the phosphor host transfers energy to the excited state $^5D_4$ of Eu^{3+} ions, resulting in characteristic Eu^{3+} emissions. When Dy^{3+} ions in the phosphor structure are excited at 352 nm, they transition from the $^6H_{15/2}$ ground state to the $^6P_{7/2}$ excited state. This is followed by non-radiative transitions to the $^4F_{9/2}$ energy level. From this level, characteristic Dy^{3+} emissions at 480 nm (blue), 575 nm (yellow) and 665 nm

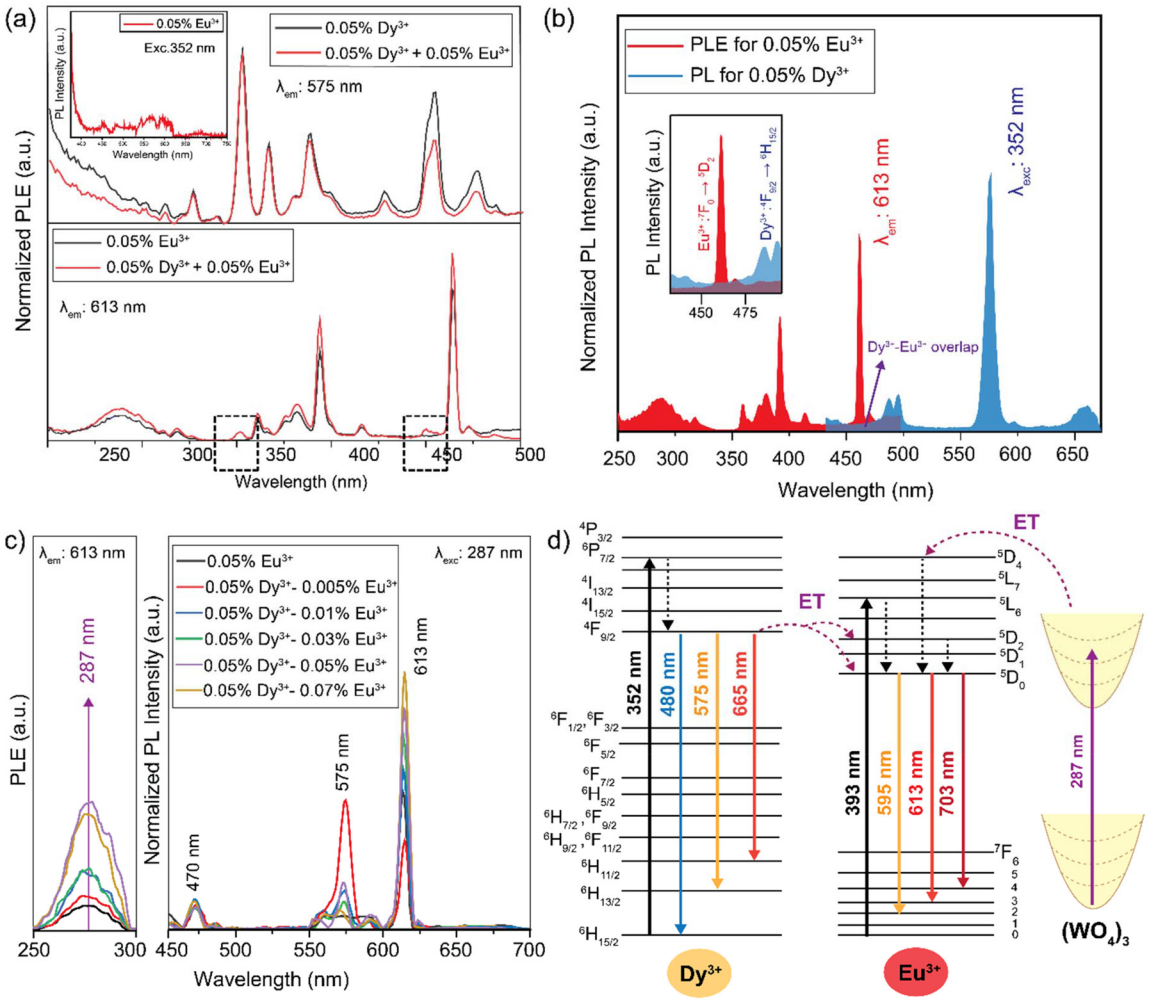

Fig. 5 PLE spectra of (a) (top) NCGW:0.05%Dy^{3+} single-doped and NCGW:0.05%Dy^{3+}–0.05%Eu^{3+} co-doped phosphors monitored under typical Dy^{3+} emission at 575 nm (Inset of Fig. 5a illustrates PL emission graph for NCGW:0.05%Eu^{3+} sample at 352 nm excitation) and (bottom) NCGW:0.05%Eu^{3+} single-doped and NCGW:0.05%Dy^{3+}–0.05%Eu^{3+} co-doped phosphors monitored under typical Eu^{3+} emission at 613 nm. (b) Overlap diagram of excitation and emission spectra of Dy^{3+} and Eu^{3+}. (c) (left) PLE spectra of NCGW:0.05%Eu^{3+} and NCGW:0.05%Dy^{3+}–*y*Eu^{3+} phosphors under typical Eu^{3+} emission at 613 nm and (right) PL spectra under 287 nm excitation. (d) Schematic representation of the energy level diagram highlighting the possible energy transfer process between Dy^{3+} and Eu^{3+} ions in NCGW phosphor.

(red) are observed as the ions return to the $^6H_{15/2}$ ground state. Upon excitation at 393 nm, Eu^{3+} ions transition from the $^7F_0$ ground state to the $^5L_6$ excited state. They then undergo non-radiative transitions to the $^5D_0$ energy level, resulting in characteristic Eu^{3+} emissions at 595 nm (orange), 613 nm (red) and 703 nm (far-red) as they return to the ground state. Additionally, the excitation of Dy^{3+} ions at 352 nm can result in energy transfer to the $^5D_0$ and $^5D_2$ energy levels of Eu^{3+} ions, which are proximate to the excited $^4F_{9/2}$ energy level of Dy^{3+} ions. Consequently, characteristic emission peaks of Eu^{3+} ions are observed upon 352 nm excitation, indicating a unidirectional energy transfer from Dy^{3+} to Eu^{3+} ions.

3.5. Thermal stability analysis and pc-WLED studies

Phosphors with exceptional thermal stability are essential for indoor lighting, as the operating temperature of typical WLEDs can rise up to 150 °C, with the 20 °C to 60 °C range reflecting more moderate thermal conditions commonly encountered in everyday applications.[42] It is essential for these phosphors to maintain their luminescence intensity and colorimetric properties at elevated temperatures. To assess this, the temperature-dependent PL spectra of the selected NCGW:0.05%Dy^{3+}–0.05%Eu^{3+} co-doped phosphor are recorded and illustrated in Fig. 6a and b, monitoring the 575 nm emission of Dy^{3+} under 352 nm excitation and the 613 nm emission of Eu^{3+} under 393 nm excitation, respectively. The intensities of the 573 nm and 613 nm emission bands decrease due to thermal quenching as the temperature increases from 25 °C to 200 °C.

The thermal stability of luminescent color was assessed by analyzing the intensity variations of red and yellow emissions between 25 °C and 75 °C, which reflects the typical operating

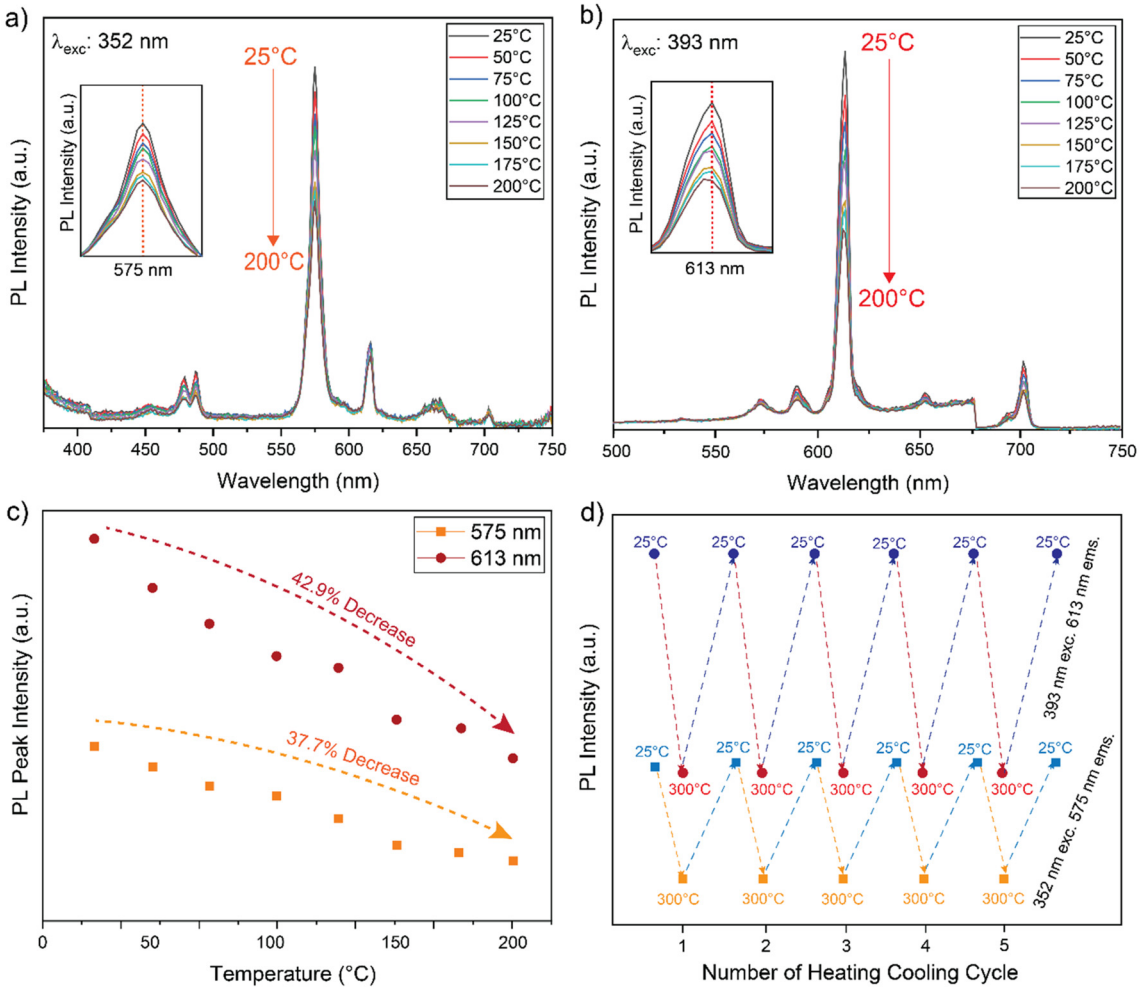

Fig. 6 Temperature-dependent PL emission spectra for the selected NCGW:0.05%Dy^{3+}–0.05%Eu^{3+} co-doped phospor from 25 °C to 200 °C: (a) under 352 nm excitation to monitor 575 nm emission of Dy^{3+}, (b) under 393 nm excitation to monitor 613 nm emission of Eu^{3+}, (c) change in PL peak intensities at 575 nm for Dy^{3+} and 613 nm for Eu^{3+} emissions under 352 nm and 393 nm excitations, respectively, (d) heating–cooling cycles (Insets of Fig. 1a and b show the temperature dependence of the maximum intensity peak position at 575 nm under 352 nm excitation and peak position at 613 nm under 393 nm excitation, respectively.).

temperature range for LEDs. Specifically, the red emission intensity decreased by approximately 20%, while the yellow emission decreased by around 12% over this range. This differential decrease suggests a slight shift in the overall emission color with increasing temperature, as the red component exhibits greater temperature sensitivity compared to the yellow component.

The yellow emission band of Dy^{3+} ions retains 62.3% of its intensity at 200 °C compared to room temperature, while the red emission band of Eu^{3+} ions retains 57.1%. As shown in Fig. 6c, this phenomenon can be explained as the thermal quenching rate of Eu^{3+} is faster than that of Dy^{3+}. However, the insets of Fig. 6a and b clearly show that the emission band positions of Dy^{3+} and Eu^{3+} remain unchanged as the temperature increases to 200 °C. These results indicate that the selected phosphor can endure the typical operating temperature range of commercial LED chips, with minimal degradation in luminescent properties.

Additionally, heating–cooling cycle experiments, conducted up to five cycles from 25 °C to 200 °C, reveal that PL intensities of Dy^{3+} and Eu^{3+} ions are not significantly affected by these cycles, as shown in Fig. 6d. This suggests that the PL characteristics of the phosphor remain stable even after multiple heating–cooling cycles, demonstrating good thermal stability and supporting its suitability for use with commercial UV LED chips, where temperature fluctuations are common.

Ultimately, a proof-of-concept pc-WLED is constructed by placing the selected NCGW:0.05%Dy^{3+}–0.05%Eu^{3+} co-doped phospor on top of a commercial UV LED chip, as shown in Fig. 7a. The phosphor exhibits a PLQY of 23% (see inset of Fig. 7b), which aligns well with values reported in similar studies in the literature.[43]

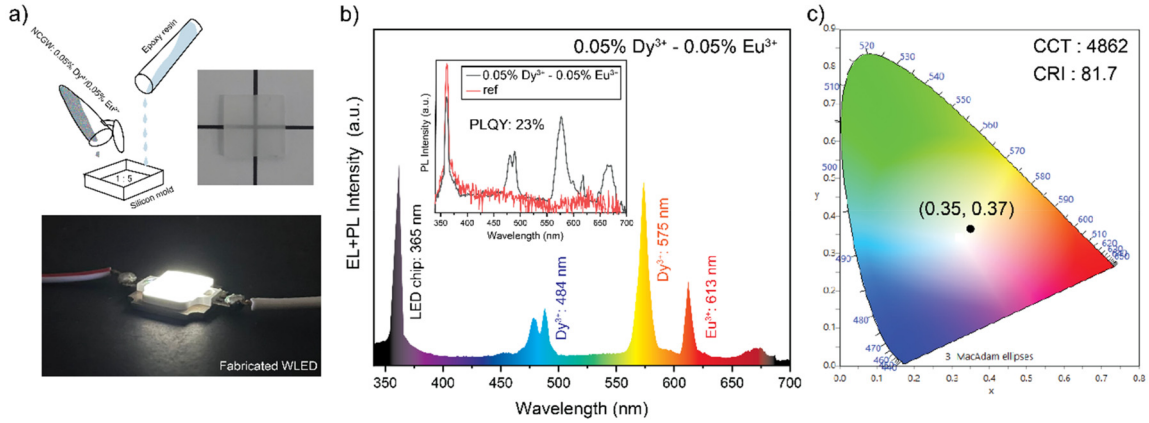

Fig. 7 (a) Design and construction of a prototype WLED using the NCGW:0.05%Dy^{3+}–0.05%Eu^{3+} co-doped phospor exhibiting white light emission on a commercial 365 nm UV LED chip, (b) emission spectra of an UV LED chip and the selected NCGW:0.05%Dy^{3+}–0.05%Eu^{3+} co-doped phospor (inset shows the PLQY measurement results under 360 nm excitation), (c) corresponding CIE chromaticity diagram with colorimetric parameters.

Table 1 Comparison of the CCT, CRI values and CIE color coordinates of selected NCGW:0.05% Dy^{3+}–0.05%Eu^{3+} co-doped phospor with previously reported studies on Dy^{3+} and Eu^{3+} doped phosphors for white light generation and commercial LEDs

Phosphor	Lanthanides	Excitation	CCT (K)	CRI	CIE coordinates	Ref.
Commercial LED	—	—	4000–6000	>80	(0.33, 0.33)	—
$KBaGd(WO_4)_3$	Dy^{3+}, Eu^{3+}	365 nm	—	73.9	(0.41, 0.39)	27
$BaLa_4Si_3O_{13}$	Dy^{3+}, Eu^{3+}	370 nm	4285	83.3	—	28
$NaCaGd(WO_4)_3$	(BAM:Eu^{2+}), 0.6Tb^{3+},0.1Eu^{3+}	365 nm	4505	87.3	(0.36, 0.38)	31
$Ca_3YAl_3B_4O_{15}$	Dy^{3+}, Eu^{3+}	365 nm	4109		(0.36, 0.32)	44
$Li_3Ba_2Gd_{2.88}(MoO_4)_8$	Dy^{3+}, Eu^{3+}	385 nm	6212		(0.33, 0.19)	45
$CaBi_2Nb_2O_9$	Dy^{3+}, Eu^{3+}	365 nm	5472	78.7	(0.33, 0.35)	46
$Ca_7Mg_2(PO_4)_6$	Dy^{3+}, Eu^{3+}	365 nm	3878	86.7	(0.38, 0.37)	47
$Na_3Ca_4(TeO_3)(PO_4)_3$	$BaMgAl_{10}O_{17}$:Eu^{2+}, $(Ba,Sr)_2SiO_4$:Eu^{2+},Dy^{3+}, Eu^{3+}	365 nm	4399	94.9	(0.37, 0.37)	48
$SrLaLiTeO_6$	Dy^{3+}, Eu^{3+}	350 nm	3232	86.5	(0.37, 0.35)	49
$MgAl_2O_4$	Dy^{3+}, Eu^{3+}	351 nm	6494	—	(0.31, 0.33)	50
$NaCaGd(WO_4)_3$	Dy^{3+}, Eu^{3+}	365 nm	4862	81.7	(0.35, 0.37)	Present work

Under the excitation of the LED chip at 365 nm, different emission bands are observed from Dy^{3+} ions (484 and 575 nm) and Eu^{3+} ions (613 nm) (Fig. 7b). The constructed WLED emits across almost the entire visible spectrum without interruptions, demonstrating promising color properties with CIE color coordinates of x = 0.35 and y = 0.37, which are quite close to pure white light coordinates. It also has a CCT value of 4862 K, approximating cool daylight. Additionally, the relatively broad emission bands of the Eu^{3+}/Dy^{3+} co-doped NCGW phosphor result in a high CRI value of 81.7 (Fig. 7c).

Table 1 lists the colorimetric properties (CCT, CRI values and CIE color coordinates) of selected NCGW:0.05%Dy^{3+}–0.05%Eu^{3+} co-doped phospor coupled with a commercial 365 nm UV LED chip, compared with previously reported Dy^{3+} and Eu^{3+} doped phosphors for white light generation and commercial LEDs. It is evident that the selected NCGW:0.05% Dy^{3+}–0.05%Eu^{3+} co-doped phospor exhibits either comparable or superior colorimetric values to those reported in previous research, which has important implications for the future of indoor lighting applications. The ability of these phosphors to deliver high-quality white light with enhanced color rendering and efficiency makes them crucial for the development of next-generation pc-WLEDs.

4. Conclusions

In conclusion, we successfully synthesize and characterize color-tunable NCGW phosphors co-doped with Dy^{3+} and Eu^{3+} ions, demonstrating their potential for application in pc-WLEDs. Through various analyses, including X-ray diffraction, Rietveld refinement, and scanning electron microscopy, we confirm the phase purity and morphology of the synthesized phosphors. Photoluminescence studies under 352 nm and 393 nm excitations reveal efficient energy transfer between Dy^{3+} and Eu^{3+} ions, enabling tunable emission properties. Remarkably, the characteristic emission peaks of Dy^{3+} and Eu^{3+} ions remain stable at elevated temperatures up to 200 °C, showcasing robust chromatic stability. Despite thermal quenching effects, the phosphors retain a significant portion of their initial emission intensity. The proof-of-concept WLED prototype, utilizing a single-phase NCGW:0.05%Dy^{3+}–0.05%

Eu^{3+} phosphor and a 365 nm UV chip, demonstrates impressive colorimetric performance with a color rendering index of 81.7, a correlated color temperature of 4862 K, and CIE chromaticity coordinates of (0.35, 0.37). These results highlight the potential of Dy^{3+} and Eu^{3+} co-doped NCGW phosphors for full-spectrum WLED applications. These advancements could lead to more energy-efficient, cost-effective, and environmentally friendly lighting solutions, thereby revolutionizing the lighting industry and contributing to global sustainability efforts.

Author contributions

Utku Ekim: investigation, visualization, writing – original draft, writing – review & editing, validation. Ikhlas Kachou: investigation, validation. Tarak Kallel: investigation, validation. Mohamed Dammak: conceptualization, investigation, validation, supervision, writing – review & editing. Miray Çelikbilek Ersundu: writing – original draft, writing – review & editing, validation, supervision, project administration. Ali Erçin Ersundu: conceptualization, methodology, writing – original draft, writing – review & editing, validation, supervision, project administration, funding acquisition.

Data availability

The data supporting this article are available within the main article.

Conflicts of interest

The authors declare no competing financial interest.

Acknowledgements

This work was supported by Yildiz Technical University Scientific Research Projects Coordination Unit under project number FBA-2024-6319.

References

1 Y. Fu, X. Wang and M. Peng, *J. Mater. Chem. C*, 2020, **8**, 6079–6085.
2 Y. Xue, Y. Liang, Y. Dou, H. Li, Q. Wang, X. Wu and Y. Han, *J. Alloys Compd.*, 2023, **940**, 168917.
3 W. Yan, Y. Wei, M. S. Molokeev, S. Wang and G. Li, *J. Alloys Compd.*, 2022, **908**, 164621.
4 P. S. Babu, P. P. Rao and T. S. Sreena, *J. Mater. Sci.: Mater. Electron.*, 2019, **30**, 16174–16183.
5 P. Dai, X. Zhang, L. Bian, S. Lu, Y. Liu and X. Wang, *J. Mater. Chem. C*, 2013, **1**, 4570.
6 M. Peng, X. Yin, P. A. Tanner, M. G. Brik and P. Li, *Chem. Mater.*, 2015, **27**, 2938–2945.
7 W. B. Im, N. George, J. Kurzman, S. Brinkley, A. Mikhailovsky, J. Hu, B. F. Chmelka, S. P. DenBaars and R. Seshadri, *Adv. Mater.*, 2011, **23**, 2300–2305.
8 L. Wang, R.-J. Xie, T. Suehiro, T. Takeda and N. Hirosaki, *Chem. Rev.*, 2018, **118**(4), 1951–2009.
9 S. Pimputkar, J. S. Speck, S. P. DenBaars and S. Nakamura, *Nat. Photonics*, 2009, **3**, 180–182.
10 P. Pust, P. J. Schmidt and W. Schnick, *Nat. Mater.*, 2015, **14**, 454–458.
11 S.-P. Lee, T.-S. Chan and T.-M. Chen, *ACS Appl. Mater. Interfaces*, 2015, **7**, 40–44.
12 H. Daicho, T. Iwasaki, K. Enomoto, Y. Sasaki, Y. Maeno, Y. Shinomiya, S. Aoyagi, E. Nishibori, M. Sakata, H. Sawa, S. Matsuishi and H. Hosono, *Nat. Commun.*, 2012, **3**, 1132.
13 K.-W. Huang, W.-T. Chen, C.-I. Chu, S.-F. Hu, H.-S. Sheu, B.-M. Cheng, J.-M. Chen and R.-S. Liu, *Chem. Mater.*, 2012, **24**, 2220–2227.
14 X. Li, J. D. Budai, F. Liu, J. Y. Howe, J. Zhang, X.-J. Wang, Z. Gu, C. Sun, R. S. Meltzer and Z. Pan, *Light: Sci. Appl.*, 2013, **2**, e50.
15 Z. Yang, G. Liu, Y. Zhao, Y. Zhou, J. Qiao, M. S. Molokeev, H. C. Swart and Z. Xia, *Adv. Opt. Mater.*, 2022, **10**, 2102373.
16 L. Jiang, X. Jiang, Y. Zhang, C. Wang, P. Liu, G. Lv and Y. Su, *ACS Appl. Mater. Interfaces*, 2022, **14**, 15426–15436.
17 K. Zhao, L. Yin, Z. Ma, T. Yang, H. Tang, P. Cao and S. Huang, *Inorg. Chem.*, 2022, **61**, 1627–1635.
18 B. Wang, H. Lin, J. Xu, H. Chen and Y. Wang, *ACS Appl. Mater. Interfaces*, 2014, **6**, 22905–22913.
19 Y. Cai, Y. Yang, H. Liu, N. Song, H. He and J. Wang, *Inorg. Chem.*, 2022, **61**, 8529–8539.
20 Y. Wang, G. Zhu, S. Xin, Q. Wang, Y. Li, Q. Wu, C. Wang, X. Wang, X. Ding and W. Geng, *J. Rare Earths*, 2015, **33**, 1–12.
21 C. C. Lin and R.-S. Liu, *J. Phys. Chem. Lett.*, 2011, **2**, 1268–1277.
22 S. Liu, J. He, Z. Wu, J. H. Jeong, B. Deng and R. Yu, *J. Lumin.*, 2018, **200**, 164–168.
23 P. Dang, S. Liang, G. Li, H. Lian, M. Shang and J. Lin, *J. Mater. Chem. C*, 2018, **6**, 9990–9999.
24 N. Wang, W. Zhao, J. Chen, J. Wang, Y. Meng, S. Yi and Y. Zhu, *J. Mater. Sci.: Mater. Electron.*, 2016, **27**, 6681–6689.
25 Y. Zhang, X. Zhang, H. Zhang, L. Zheng, Y. Zeng, Y. Lin, Y. Liu and B. Lei, *RSC Adv.*, 2018, **8**, 3530–3535.
26 H. Zhou, Y. Jin, M. Jiang, Q. Wang and X. Jiang, *Dalton Trans.*, 2015, **44**, 1102–1109.
27 W. Zhou, M. Song, Y. Zhang, Z. Xie and W. Zhao, *Opt. Mater.*, 2020, **109**, 110271.
28 F. Liao, B. Shen, W. Wu, Y. Zhang and J. Hu, *Ind. Eng. Chem. Res.*, 2021, **60**, 2931–2943.
29 S. Hariyani and J. Brgoch, *Chem. Mater.*, 2020, **32**, 6640–6649.
30 X. Wang, G. Li, Y. Wei and X. Guan, *Chin. J. Inorg. Chem.*, 2020, **36**, 1881–1890.

31 J. Xie, L. Cheng, H. Tang, Z. Wang, H. Sun, L. Lu, X. Mi, Q. Liu and X. Zhang, *Inorg. Chem. Front.*, 2021, **8**, 4517–4527.
32 H. Najafi-Ashtiani, A. Bahari, S. Gholipour and S. Hoseinzadeh, *Appl. Phys. A*, 2018, **124**, 24.
33 M. Zhu, C. Hu, J. Li, Y. Feng, H. Kong, S. Ullah, M. Li, F. You, B. Teng, D. Zhong and J. Tang, *J. Mater. Sci.: Mater. Electron.*, 2018, **29**, 20607–20614.
34 T. Jeyakumaran, N. Venkatesh Bharathi, R. Shanmugavel, P. Sriramachandran and S. Ramaswamy, *J. Inorg. Organomet. Polym. Mater.*, 2021, **31**, 695–703.
35 T. T. Deng, E. H. Song, J. Sun, L. Y. Wang, Y. Deng, S. Ye, J. Wang and Q. Y. Zhang, *J. Mater. Chem. C*, 2017, **5**, 2910–2918.
36 Y. Liu, J. Silver, R.-J. Xie, J. Zhang, H. Xu, H. Shao, J. Jiang and H. Jiang, *J. Mater. Chem. C*, 2017, **5**, 12365–12377.
37 M. Yu, J. Lin, Z. Wang, J. Fu, S. Wang, H. J. Zhang and Y. C. Han, *Chem. Mater.*, 2022, **14**, 2224–2231.
38 G. Blasse, *Phys. Lett. A*, 1968, **28**, 444–445.
39 J. C. Wright, Up-conversion and excited state energy transfer in rare-earth doped materials, in *Radiationless Processes in Molecules and Condensed Phases*, ed. F. K. Fong, Springer-Verlag Berlin Heidelberg, Berlin, Heidelberg, 1976, pp. 239–295.
40 G. Blasse, *Prog. Solid State Chem.*, 1988, **18**, 79–171.
41 M. Vijayakumar and K. Marimuthu, *J. Lumin.*, 2016, **178**, 414–424.
42 I. Beliakova, L. Kostyk, P. Maruschak, V. Medvid, V. Piscio, O. Shovkun and R. Mykhailyshyn, *Appl. Sci.*, 2024, **14**, 5678.
43 R. V. Deun, D. Ndagsi, J. Liu, I. V. Driessche, K. V. Hecked and A. M. Kaczmarek, *Dalton Trans.*, 2015, **44**, 15022–15030.
44 S. Liu, L. Zeng, Z. Zhao, M. Deng, X. Wang and W. Zhang, *Ceram. Int.*, 2022, **48**, 36706–36714.
45 H. Ye, Z. Liu, W. Zhang, W. Xie, Z. Feng, Y. Ye, Y. Chen and X. Sheng, *Polyhedron*, 2024, **260**, 117063.
46 Q. Ren, K. Liu, X. Wu and O. Hai, *Mater. Today Commun.*, 2024, **38**, 108519.
47 L. Chen, W. Zhang, H. Zhu, J. Li, Q. Li, W. Zhao, Y. Yang and D. S. Li, *Ceram. Int.*, 2024, **50**, 7101–7109.
48 R. Song, Z. Yang, H. Zhang, X. Tang, Y. Liu and J. Zhu, *Ceram. Int.*, 2023, **49**, 22323–22331.
49 J. S. Gong, W. B. Dai, J. Luo, K. Nie and M. Xu, *Ceram. Int.*, 2023, **49**, 31024–31034.
50 K. Panigrahi, S. Saha, S. Sain, R. Chatterjee, A. Das, U. K. Ghorai, N. Sankar Das and K. K. Chattopadhyay, *Dalton Trans.*, 2018, **47**, 12228–12242.